Novel Topological Insulators with Hybrid-order Boundary States

Yan-Qing Zhu,[1,2,*] Zhen Zheng,[3,4] Giandomenico Palumbo,[5,†] and Z. D. Wang[1,2,‡]

[1] *Guangdong-Hong Kong Joint Laboratory of Quantum Matter, Department of Physics, and HK Institute of Quantum Science & Technology, The University of Hong Kong, Pokfulam Road, Hong Kong, China*

[2] *Quantum Science Center of Guangdong-Hong Kong-Macau Great Bay Area, 3 Binlang Road, Shenzhen, China*

[3] *Key Laboratory of Atomic and Subatomic Structure and Quantum Control (Ministry of Education), Guangdong Basic Research Center of Excellence for Structure and Fundamental Interactions of Matter, School of Physics, South China Normal University, Guangzhou 510006, China*

[4] *Guangdong Provincial Key Laboratory of Quantum Engineering and Quantum Materials, Guangdong-Hong Kong Joint Laboratory of Quantum Matter, Frontier Research Institute for Physics, South China Normal University, Guangzhou 510006, China*

[5] *School of Theoretical Physics, Dublin Institute for Advanced Studies, 10 Burlington Road, Dublin 4, Ireland*

(Dated: May 1, 2024)

We report the discovery of several classes of novel topological insulators (TIs) with hybrid-order boundary states generated from the first-order TIs with additional crystalline symmetries. Unlike the current studies on hybrid-order TIs where different-order topology arises from merging different-order TIs in various energy, these novel TIs exhibit a remarkable coexsitence of first-order gapless modes and higher-order Fermi-arc states, behaving as a hybrid between the first-order TIs and higher-order topological semimetals within a single bulk gap. Our findings establish a profound connection between these novel d-dimensional (dD) TIs and $(d-1)$D higher-order TIs (HOTIs), which can be understood as a result of stacking $(d-1)$D HOTIs to dD with $d = 3, 4$, revealing unconventional topological phase transitions by closing the gap in certain first-order boundaries rather than the bulk. The bulk-boundary correspondence between these higher-order Fermi-arcs and bulk topological invariants acsossiated with additional crystallline symmetries is also demonstrated. We then discuss the conventional topological phase transitions from these novel TIs to nodal-line/nodal-surface semimetal phases, where the gapless phases host new kinds of topological responses. Meawhile, we present the corresponding topological semimetal phases by stacking these unique TIs. Finally, we discuss potential ways to realize these novel phases in synthetic and real materials, with a particular focus on the feasible implementation in optical lattices using ultracold atoms.

Introduction.— Topological insulators (TIs) and topological semimetals (TSMs) have emerged as one of the most active fields of modern physics over the past two decades [1–3], attracting significant attention from researchers in condensed matter physics and artificial systems[4–10]. One significant property of topological phases is the presence of bulk-boundary correspondence, which guarantees the existence of gapless first-order boundary modes that are associated with certain bulk topological invariant. These first-order topological materials have been classifed within the framework provided by the real K-theory [11] and Altland-Zirnbauer (AZ) classes [12] for both gapped [13, 14] and gapless [15–17] systems, based on their fundamental symmetries including time-reversal $\mathcal{T}$, charge-conjugation $\mathcal{C}$, and chiral symmetry $\mathcal{S}$.

Recent research focus has been extended to higher-order topological phases with additional crystalline symmetries [18–22]. These systems do not feature first-order even second-order boundary gapless states but instead exhibit gapless states at higher-order boundaries. For instance, a second-order TI (SOTI) in 3D hosts boundary gapless modes at 1D hinges (i.e., second-order boundary) while its 2D surface (i.e., first-order boundary) spectrum is gapped. By further gapping the gapless hinge states, a 3D third-order TI (TOTI) can be induced, leading to the existence of zero-energy modes at 0D corners (i.e., third-order boundary). By stacking these HOTIs along an extra dimension, one can obtain higher-order TSMs (HOTSMs) with higher-order Fermi-arcs [23–26]. Moreover, hybrid-order TIs [27] with multi-gaps have been also discovered in metamaterials [28–30], which simultaneously host hybrid-order topological boundary modes under different open boundary conditions (OBCs) in various energy. Building on recent advancements in the aforementioned areas, a natural question arises: *Are there novel types of TIs that host hybrid-order boundary modes within a single bulk gap? Can we establish bulk-boundary correspondence in these phases?*

In this Letter, we answer these questions positively. We introduce several novel classes of TIs that exhibit unique hybrid-order boundary states consisting of both first-order gapless modes and higher-order Fermi-arc states within a single bulk gap, which can be seen as a hybrid between first-order TIs (FOTIs) and HOTSMs. These phases can be simply generated from the first-order TIs (FOTIs) by shifting the gapless modes in first-order boundary Brillouin Zone (BZ) through specific perturbations protected by crystalline symmetries. On the other hand, we can also regard these unique TI phases in dD as the stacking $(d-1)$D HOTIs along an additional spatial dimension ($d=3,4$). In this viewpoint, we reveal unconventional topological phase transitions (UTPTs) by closing the first-order boundary gap while maintaining an open bulk gap, i.e., the unconventional phase transition points are topological crystalline insulators (TCIs) [31]. We emphasize these higher-order Fermi-arcs can be well described by the bulk topology associated with related crystalline symmetries. For concreteness, we mainly focus on several 4D models in the main text: (i) Class A with combined mirror symmetry; (ii) Class AIII with $\mathcal{RT}$-symmetry ; (iii) Class A with $C_4\mathcal{T}$-symmetry; (iv) Class AIII with $C_4\mathcal{T}$-symmetry. In (i), we find a 4D TI hosts both first-order boundary Weyl cones and second-order chiral hinge Fermi-arcs located at the typical hinges determined by the related mirror reflection symmetries; In (ii), a 4D TI with spin conservation hosts first-order boundary Dirac cones and second-order helical hinge Fermi-arcs while Dirac cones will be expanded into real Dirac nodal-lines and helical hinge states will be gapped leading to third-order Fermi-arcs after introducing a spin-orbit-coupling (SOC) $\mathcal{RT}$-symmetry perturbation; In (iii), a 4D TI with $C_4\mathcal{T}$ is similar to the case (i) but with the difference that the second-order hinge Fermi-arc are always located at four hinges determined by more combined mirror-symmetries; (iv) Two copies of Hamiltonian with opposite sign in (iii) are considered which supports first-order boundary Dirac cones and second-order helical hinge Fermi-arcs. By performing dimensional reduction with $k_z=0$, the corresponding 3D models and physical pictures are obtained, which are presented in the Supplemental Materials (SM). The explicit expressions of the topological numbers associated with the corresponding crystalline symmetries are presented. Moreover, we also explore the conventional topological phase transition (CTPT) from a novel TI in case (i)/(ii) to a nodal-line/nodal-sphere phase, presenting the topological response theory of these gapless phases. Furthermore, we discuss the related topological semimetal phases by stacking these novel TIs along an additional spatial dimension. Finally, we discuss the possible ways to realize these novel phases in synthetic and real materials, including the implemented proposals in optical lattices using ultracold atoms.

Four-band model in Class $A^{\mathcal{M}_{ij}}$.— We now consider a 4D four-band model with its Bloch Hamiltonian given by,

$$\mathcal{H}_1(\boldsymbol{k}) = \mathcal{H}_0 + \Delta_1, \tag{1}$$

where $\mathcal{H}_0 = \sum_i d_i\Gamma_i + d_0\Gamma_0$ with the Bloch vector $d_i = \sin k_i$, $d_0 = M - \sum_i \cos k_i$ ($i=x,y,z,w$). The perturbation $\Delta_1 = b_{xw}\Gamma_0\Gamma_{14} + b_{yw}\Gamma_0\Gamma_{24}$. Here the Driac matrices are $\Gamma_1 = G_{31}$, $\Gamma_2 = G_{32}$, $\Gamma_3 = G_{33}$, $\Gamma_4 = G_{20}$, $\Gamma_0 = G_{10}$, $\Gamma_{ab} = \frac{i}{2}[\Gamma_a, \Gamma_b]$, and satisfy $\{\Gamma_i, \Gamma_j\} = 2\delta_{ij}$. We mix the notation $i \in (1,2,3,4) \leftrightarrow (x,y,z,w)$ in the subscript of Γ_i and label $G_{ab} = \sigma_a \otimes \sigma_b$ through the 2×2 identity σ_0 and Pauli matrices σ_i hereafter. As one can see that $\mathcal{H}_0$ is the well-known 4D quantum Hall insulator (QHI) characterized by the second Chern number (SCN) C_2 [32], harboring $|C_2|$ Weyl cones at the origin of the 3D boundary BZ [33]. Under OBCs along the x (w)-direction with a chain length L, introducing a non-zero b_{xw} term in $\mathcal{H}_0$ leads to the shifted Weyl cones along the k_w (k_x)-axis in the boundary BZ, resulting in the second-order chiral Fermi-arc hinge states when considering OBCs at x and y directions. A similar effect is observed when only the b_{yw} term is non-zero, as shown in Fig. 1. We present the effective boundary Hamiltonian and numeric results in the SM [34].

In what follows we discuss the topology of this system. The initial Hamiltonian $\mathcal{H}_0(\boldsymbol{k})$ in class AII respects $\mathcal{T}$ represented as $\hat{\mathcal{T}} = \Gamma_{13}\mathcal{K}$, where $\mathcal{K}$ is the complex conjugate. In addition, $\mathcal{H}_0$ preserves extra crystalline symmetries, including inversion symmetry $\mathcal{I}$ [35] and the combined mirror reflection symmetries $\mathcal{M}_{ij} = \mathcal{M}_i\mathcal{M}_j$, where each mirror reflection $\mathcal{M}_i$ inverts one of the momentum components k_i [36]. We present all the definitions of the corresponding crytalline symmetries in the SM [34]. For simplicity, we first consider the case when only b_{xw} term in Δ_1 is numerically small, it breaks $\mathcal{T}$ and only preserves $\mathcal{M}_{xw}$ and $\mathcal{M}_{yz}$ symmetries. The system now falls into class A and still hosts a non-trivial C_2 with the shifted first-order Weyl boundary states. To characterize the second-order topology, we can define extra topological numbers at $\mathcal{M}_{xw}/\mathcal{M}_{yz}$-invariant points $\Lambda_a^{xw}/\Lambda_a^{yz}$ [37], i.e., named "*mirror first Chern number*" (MFCN),

$$C_{1m}^{ij}(\Lambda_a^{ij}) = [C_{+i}(\Lambda_a^{ij}) - C_{-i}(\Lambda_a^{ij})]/2, \tag{2}$$

where $C_{\pm i}$ denotes the first Chern number defined in 2D subsystems $\mathcal{H}_1^{\Lambda_a^{ij}}(k_l, k_m)$ of the eigenspace $\mathcal{E} = \pm i$ of $\hat{\mathcal{M}}_{ij}$ [36]. For simplicity and without loss of generality, we focus on the case when M near 3 hereafter, evaluation shows that $C_{1m}^{xw} = -1/C_{1m}^{yz} = 1$ at $\Lambda_1^{xw}/\Lambda_1^{yz} = (0,0)$, and $C_{1m}^{xw}(\Lambda_a^{xw}) = 0/C_{1m}^{yz}(\Lambda_a^{yz}) = 0$ for the rest of the three $\Lambda_a^{xw/yz}$ points [34]. These results establish the bulk-hinge correspondence and provide detailed information of the chiral hinge Fermi-arcs, as depicted in Fig. 1(a). Since these hinge Fermi-arcs are formed by stacking the 1D chiral modes $\mathcal{H}_{R/L} = \pm k_z$ along k_w axis, once $\mathcal{M}_{xw}$ acts on one of hinge states, it will transform this states to the mirror reflection hinge about $x=0$ and $k_w=0$ planes without changing its chirality; while $\mathcal{M}_{yz}$ tranforms one of the hinge states to its mirror-symmetric hinge about $y=0$ and then changes the chirality of this hinge mode due to the mirror reflection about $k_z=0$ plane, causing $\pm k_z \to \mp k_z$. Similar picture also appear when M is in other parameter regions[34]. When only b_{yw} is non-zero, the system preserves both $\mathcal{M}_{xz}$ and $\mathcal{M}_{yw}$ symmetries describing the existence of second-order chiral Fermi-arcs, as depicted in Fig. 1 (b).

When both b_{xw} and b_{yw} survive, $\mathcal{M}_{xw}$ and $\mathcal{M}_{yz}$ are broken. For the typical case when $b_{xw} = b_{yw}$, $\mathcal{H}_1$ hosts an extra combined symmetry $\mathcal{M}_{(x-y)z} = \mathcal{M}_{x-y}\mathcal{M}_z$ with $\mathcal{M}_{x-y}$ being the mirror reflection about the mirror-invariant line $k_x = k_y$[38]. In the same spirit, we can calculate the MFCNs $C_{1m}^{k_z}$ at $k_x = k_y$, $k_z = 0, \pi$ planes with $C_{1m}^{0} = -1$ and $C_{1m}^{\pi} = 0$[34]. As we can see that chiral Fermi-arcs are located at diagonal hinges with mirror reflection about $x = y$ plane harboring opposite chirality due to the operation of $\mathcal{M}_z$, as shown in Fig. 1(c). Similarly, when $b_{xw} = -b_{yw}$, $\mathcal{H}_1$ preserves $\mathcal{M}_{(x+y)z}$ symmetry with $C_{1m}^{0} = 1$ and $C_{1m}^{\pi} = 0$, enforcing the location of Fermi-arcs at anti-diagonal corners with opposite chirality[34]. If $b_{xw} \neq |b_{yw}|$, Δ_1 breaks $\mathcal{T}$ and all the $\mathcal{M}_{ij}$-symmetries. However, the system still hosts the $\mathcal{I}$-symmetry which guarantees the second-order Fermi-arc states as a superposition of the cases where either $b_{yw} = 0$ or $b_{xw} = 0$. We emphasize that $\mathcal{M}_{ij}$-symmetry is used to construct this unique TI; it is itself not essential for the existence of second-order hinge Fermi-arcs. The hinge states are robust against a $\mathcal{M}_{ij}$-symmetry breaking perturbation, as long as the bulk gap is not closed.

To understand this 4D novel phase with both first- and second-order boundary states, we can treat k_w as a parameter in this $\mathcal{H}_1$. The 3D subsystem $\mathcal{H}_1^{k_w}(k_x, k_y, k_z)$ goes through UTPTs while the gap closing happens in certain 2D surface BZs instead of the 3D bulk when tuning k_w from $-\pi$ to π. For instance and when $b_{xw} > 0$, the 3D subsystems exhibit two distinct phases, which are normal insulators for $k_w \in (-\pi, -b_{xw}) \cup (b_{xw}, \pi)$, and chiral SOTIs for $k_w \in (-b_{xw}, 0) \cup (0, b_{xw})$. The TCIs [31] at $k_w = 0, \pm b_{xw}$ serve as the unconventional transition points between these two phases, as illustrated in Fig. 1(d). Thus this novel 4D TI phase $\mathcal{H}_1$ is nothing but the stacking layers of 3D chiral SOTIs, revealing UTPTs by tuning k_w. We present detailed discussions about the topology of these 3D subsystems in the SM[34]. On the other hand, a 3D novel TI with hybrid-order boundary states can be simply obtained by setting $k_z = 0$, the system restores $\mathcal{S}$-symmetry and thus falls into class AIII. Similar discussions can be found in the SM[34].

Eight-band model in Class AIII$^{\mathcal{RT}}$ without and with SOC.— We now consider a 4D eight-band model, its Hamiltonian is given by,

$$\mathcal{H}_2(\boldsymbol{k}) = \tilde{\mathcal{H}}_0 + \Delta_2 + \Delta_3, \tag{3}$$

where $\tilde{\mathcal{H}}_0 = \sum_i d_i \tilde{\Gamma}_i + d_0 \tilde{\Gamma}_0$ with the Bloch vector d_i ($i = x, y, z, w$) are the same as in $\mathcal{H}_0$, the perturbations $\Delta_2 = b_{xw}\tilde{\Gamma}_0\tilde{\Gamma}_{14} + b_{yw}\tilde{\Gamma}_0\tilde{\Gamma}_{24} + b_{zw}\tilde{\Gamma}_0\tilde{\Gamma}_{34}$, and $\Delta_3 = c_x\tilde{\Gamma}_{61} + c_z\tilde{\Gamma}_{63}$. Here $\tilde{\Gamma}_1 = G_{331}$, $\tilde{\Gamma}_2 = G_{332}$, $\tilde{\Gamma}_3 = G_{333}$, $\tilde{\Gamma}_4 = G_{320}$, $\tilde{\Gamma}_0 = G_{310}$, $\tilde{\Gamma}_6 = G_{100}$, $\tilde{\Gamma}_7 = G_{200}$, and $\tilde{\Gamma}_{ab} = \frac{i}{2}[\tilde{\Gamma}_a, \tilde{\Gamma}_b]$. Label $G_{ijk} = \sigma_i \otimes \sigma_j \otimes \sigma_k$ hereafter. $\tilde{\mathcal{H}}_0$ is just a 4D quantum spin Hall insulator as two copies of 4D QHIs $\pm\mathcal{H}_0$ with opposite $\pm C_2$ implying the existence of 3D first-order

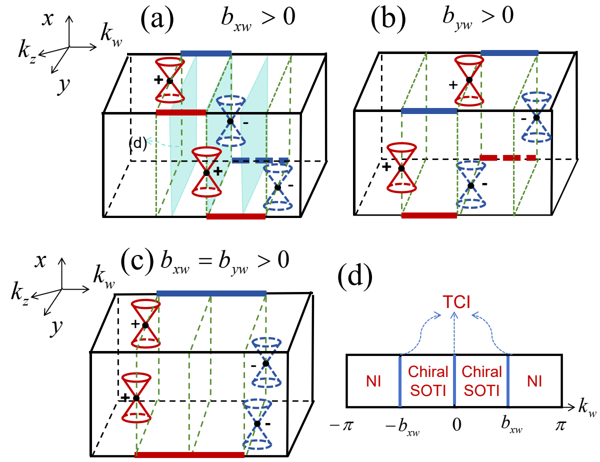

FIG. 1. Schematic of the boundary states of $\mathcal{H}_1$ with $C_2 = -1$ when $2 < M < 4$. Each first-order 3D boundary hosts a 3D Weyl cone marked in red/blue carrying right-/left-chirality while the 1D chiral hinge modes are also marked in the same way. (a) b_{xw} term shifts the Weyl cone along the k_w direction, causing it to be located at $\mathbf{k}_{x+} = (k_y, k_z, k_w) = (0, 0, b_{xw})$ at $x = -L/2$, while the Weyl cone at $x = L/2$ is shifted and located at $\mathbf{k}_{x-} = (0, 0, -b_{xw})$. If we further open the boundary along the y axis, there will be 1D chiral zero-energy Fermi-arcs located at the symmetry-protected hinges for $k_z = 0$. (b) b_{yw} term shifts the Weyl cone at $y = -L/2$ to the position $\mathbf{k}_{y+} = (k_x, k_z, k_w) = (0, 0, b_{yw})$ and another Weyl cone at $y = L/2$ to $\mathbf{k}_{y-} = (0, 0, -b_{yw})$. 1D chiral hinge Fermi-arcs also appear at chosen hinges when OBC along x and y directions are assumed. (c) The superposition of the cases in Figs. (a) and (b) with $b_{xw} = b_{yz}$ where second-order Fermi-arcs only appear at two $\mathcal{M}_{(x-y)z}$-symmetric hinges. (d)Phase diagram of 3D subsystems $\mathcal{H}_1^{k_w}$ with only b_{xw} being non-zero by varying k_w. Here"NI" denotes the normal insulator.

boundary Dirac modes. Δ_2 shifts the gapless Dirac cones in 3D boundary momentum space similar to that case in $\mathcal{H}_0$, resulting in second-order helical Fermi-arc hinge states. Δ_3 behaves like a SOC, where c_i expands the 3D Dirac cone into a nodal line structure at $k_i = 0$ plane at the boundary normal to j-direction. For instance, non-zero c_x term expands the boundary Dirac cone into a nodal line at $k_x = 0$ plane in the case of OBC at $y/z/w$-direction[34].

In the following we discuss the topology of this model in details. In AZ classification [12], $\tilde{\mathcal{H}}_0$ falls into class CII with $\mathcal{T}$, $\mathcal{C}$ and $\mathcal{S}$ hosting a $\mathbb{Z}_2$ topology[39]. Since $\tilde{\mathcal{H}}_0$ is spin conservation with $\tilde{\Gamma}_5$-symmetry, we have $[\tilde{\Gamma}_5, \tilde{\mathcal{H}}_0] = 0$, where $\tilde{\tilde{\Gamma}}_5 = G_{300}$. We can define a $\mathbb{Z}_2$ number through the spin SCN [40] to characterize the first-order topology with bulk-boundary correspondence even if $\mathcal{T}$ and $\mathcal{C}$ will be broken later[41]. In addition, $\tilde{\mathcal{H}}_0$ also respects the following crystalline symmetries, including $\mathcal{I}$, and $\mathcal{M}_i$ leading to the combined symmetries $\mathcal{M}_{ij}$ and $\mathcal{R}_i\mathcal{T} = \mathcal{M}_i\mathcal{I}\mathcal{T}$ for $i = x, y, z, w$[42].

We first consider the situation when Δ_2 plays the role

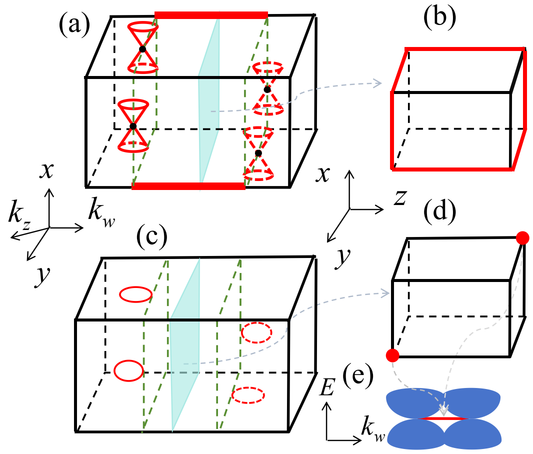

FIG. 2. Schematic of the boundary states of $\mathcal{H}_3$ when $2 < M < 4$. (a-b)$b_{xw} = b_{yw} = b_{zw} > 0$ and $c_x = c_z = 0$, the system harbors both shifted first-order Dirac points located at the same positions as in Fig. 1(c) and second-order Fermi-arcs consisting of helical hinge states (colored in orange) of 3D SOTIs stacked along k_w axis. (c-e) $b_{xw} = b_{yw} = b_{zw} > 0$ and $c_x = c_z > 0$. The system harbors both shifted first-order nodal lines and third-order Fermi-arcs consisting of zero-mode corner states of 3D TOTIs stacked along k_w axis.

in, i.e., all $c_i = 0$. Δ_2 break $\mathcal{T}$, $\mathcal{C}$, but keep $\mathcal{S}$, $\mathcal{I}$ and thus the system is now falls into calss AIII but still hosts an unchanged spin SCN. The discussion of the second-order topology associated with the spin MFCNs [43] is similar to the cases in $\mathcal{H}_1$ when only b_{xw} and b_{yw} survive[34]. To conveniently discuss third-order topology later, we focus on a TI phase with both first- and second-order boundary states with $b_{xw} = b_{yw} = b_{zw}$ for M near 3. As shown in Fig. 2(a-b), the system hosts the second-order helical Fermi-arcs where its 3D layers $\mathcal{H}_2^{k_w}$ with $k_w \in (-b_{xw}, b_{xw})$ are SOTIs with helical states propagating along $\mathcal{M}_{x-y}$, $\mathcal{M}_{y-z}$, and $\mathcal{M}_{z-x}$ symmetric hinges[44] when considering OBCs along x-, y- and z-directions. One can also define 3D mirror winding numbers to describe this second-order topology accordingly[34].

Subsequently, we turn on $c_x = c_z$ being numeric small, $\mathcal{H}_3$ remains in class AIII harboring shifted 3D $\mathbb{Z}_2$ nodal lines [45–47] on the 3D boundaries when assuming OBC along x or y directions [Fig. 2(c)]. However, helical hinge Fermi-arcs have been gapped due to Δ_3 breaks $\tilde{\Gamma}_5$ ($\mathcal{M}_{x-y}$ and $\mathcal{M}_{y-z}$ are also broken), leading to third-order Fermi-arcs along k_w axis[34], as shown in Fig. 2(c-e). In this case, even though the spin SCN is not well-defined, one can define a $\mathbb{Z}_2$ number as 4D generalization of Kane-Mele invariant [45] since $\mathcal{H}_3$ remains respect $\mathcal{R}_w\mathcal{T}$-symmetry[42]. Alternately, we can define another topological number as $\nu = \nu_0 - \nu_\pi$ mod 2 at $\mathcal{R}_w\mathcal{T}$-invariant lines $k_w = 0, \pi$ with ν_{k_w} is a topological number of the 3D real TI with $\mathcal{S}$ [48]. Calculation results show that $\nu_0 = 1$ and $\nu_\pi = 0$ for M near 3 [34]. Meanwhile, $\mathcal{H}_3$ keeps $\mathcal{M}_{(z+x)yw} = \mathcal{M}_{z+x}\mathcal{M}_y\mathcal{M}_w$[49], $\mathcal{M}_{z-x}$, and $\mathcal{I}$-symmetries. A non-trivial 1D mirror winding number $w_{1m} = 2$ defined at $k_x = -k_z$ and $(k_y, k_w) = (0, 0)$ associated with $\mathcal{M}_{(z+x)yw}$-symmetry [34] guarantees the exact location of third-order Fermi-arc with $\mathcal{M}_w$-symmetry about $k_w = 0$ consisting of a pair of zero-modes, accumulating at two $\mathcal{M}_{(z+x)y}$-symmetric [combined mirror reflection about $z = -x$ and $y = 0$ planes] corners in a 3D real space cubic spanned in (x, y, z). The bulk-corner correspondence is established here; $\mathcal{M}_{z-x}$ implies these two zero-modes live in $z = x$ plane; these Fermi-arc states are always $\mathcal{I}$-symmetric in (x, y, z, k_w) space; see Fig. 2(d-e). We emphasize that $\tilde{\Gamma}_5$ ($\mathcal{R}_w\mathcal{T}$) symmetry guarantees the existence of second (third)-order gapless Fermi arcs in class AIII, where these boundary modes are located at the positions determined by additional crystalline symmetries.

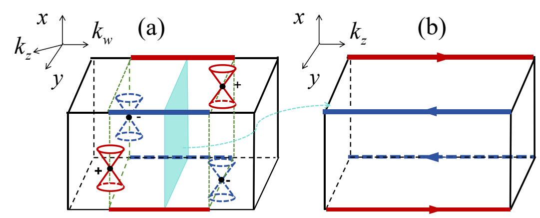

FIG. 3. Schematic of the boundary states of $\mathcal{H}_3$ when $2 < M < 4$ and $\delta > 0$ being numeric small. (a) The system harbors both shifted first-order Weyl cones [34] and the second-order chiral Fermi-arc hinge states. The green dashed squares denote the 3D TCIs being the unconventional phase transition points. (b) 3D non-trivial subsystems with fixing k_w host second-order chiral hinge states.

Four-band model in Class $A^{C_4\mathcal{T}}$ and eight-band model in Class AIII$^{C_4\mathcal{T}}$ without SOC.— We present another 4D four-band model in class A, with the Hamiltonian,

$$\mathcal{H}_3(\boldsymbol{k}) = \mathcal{H}_0 + \Delta_4, \tag{4}$$

with a perturbation $\Delta_4 = \delta(\cos k_x - \cos k_y)\Gamma_4$ breaks C_4^{zw} and $\mathcal{T}$ individually, but respects $C_4^{zw}\mathcal{T}$-symmetry [50]. As shown in Fig. 3, Δ_4 shifts the boundary Weyl cones along k_w-direction [34]. Two Weyl cones located on different boundaries [e.g. $y(x) = -L/2$ and $y(x) = L/2$] are shifted along the same direction when OBC along y (x)-direction is assumed, resulting in a second-order Fermi-arc at four hinges once we further open the boundary along x (y) axis. Except the unchanged C_2 for the first-order topolgy, we can define the so-called "*rotational spin first Chern number*" (RSFCN) at $C_4^{zw}\mathcal{T}$-invariant 2D momenta $(k_x, k_y) = (0, 0), (\pi, \pi)$ which may be used to characterize the second-order topology [34]. In addition, we can easily construct the spin conservation verion of $\mathcal{H}_3$ with eight-band as $\mathcal{H}_4(\boldsymbol{k}) = \sigma_3 \otimes \mathcal{H}_3$, which respects $C_4^{zw}\mathcal{T}$ and $\mathcal{S}$ and thus falls into class AIII. The system now hosts the first-order boundary Dirac modes and the second-order helical hinge Fermi-arcs. By setting $k_z = 0$, we obtain the corresponding 3D unique TI. All these similar discussions about the second-order topology associated with additional crystalline symmetries are presented in Ref.[34].

CTPTs and Novel TSMs.—By enlarging the parameters in Δ_1/Δ_2 of $\mathcal{H}_1/\mathcal{H}_2$, we can study the CTPT goes through a phase transition from this unique TI phase to a non-trivial nodal-line/sphere metallic phase and then finally becomes a trivial insulator. Such 4D nodal structures, including nodal-line, spin-nodal-line, and nodal-sphere, are characterized by the first Chern number (FCN) C_1, spin FCN C_{1s}, and 1D winding number w_1 respectively. The corresponding topological responses based on current works [51–53] are also discussed [34]. On the other hand, we can obtain serveral new classes of TSMs with hybrid-order boundary Fermi-arcs by stacking the above TI phases along an extra spatial dimension u, as is commonly done, i.e., $M \to M' = M - \cos k_u$, For instance, when $M = 4$, $\mathcal{H}_1(M')/\mathcal{H}_1^{k_z=0}(M')$ hosts a pair of 5D/4D nodal surfaces/lines characterized by double charges $\nu_D = (C_2/w_3, C_1)$, where w_3 denotes the 3D winding number; $\mathcal{H}_3(M')/\mathcal{H}_3^{k_z=0}(M')$ hosts a pair of hybrid-order 5D/4D monopoles characterized by C_2/w_3. Two spin copies of these nodal-structures of $\mathcal{H}_2(M')/\mathcal{H}_4(M')$ can be also extended accordingly[34].

Discussion and outlook.— In this work, we establish a valuable framework for understanding the origin of the distinctive properties of these novel TIs, demonstrating that these unique TIs can be seen as a higher-dimensional stacking effect of low-dimensional HOTIs undergoing UTPTs along an additional spatial dimension. In other words, each kind of dD HOTI corresponds to a $(d+1)$D unique TI phase for $d \geq 2$. The related nodal structures and their topological responses are also studied when $\mathcal{H}_1/\mathcal{H}_2$ becomes a gapless phase. Furthermore, the corresponding TSMs with novel nodal-structures can be obtained by stacking these TIs going through CTPTs along an extra spatial dimension. Note that these unique topological phases, especially for models with $d \geq 4$, could be experimental studied in sythetic matter, as could be realized in metamaterials[54–57], in electric circuits[58, 59], or in optical lattices with cold atoms[60–63], etc. In particular, we can utilize the cold-atom setup proposed in our previous work [41] to realize the 4D model $\tilde{\mathcal{H}}_0$ in Eq. (3), including the implementation of other models mentioned in this work in a similar manner [34]. For the 3D model in $\mathcal{H}_1$ with $k_z = 0$, $\mathcal{H}_0^{k_z=0}$ as a 3D strong TI in low-energy limit has been predicted [64] and realized [65] in real materials, such as Bi_2Se_3 and Bi_2Te_3 families, one can consider to induce Δ_1 term in these materials by magnetization or light-induced Floquet drivings [66].

We highlight that these novel topological phases can also be generalized to non-Hermitian [67, 68] and Floquet systems [69, 70]. The field-theoretical descriptions of these phases in the bulk is one of interesting directions. An intriguing and open question is the direct calculation of the effective action in the bulk. Take $\mathcal{H}_1$ as an example, the presence of shifted first-order boundary Weyl cones implies the possibility of an additional term beyond the $(4+1)$D Chern-Simons action in its 4D parent system. We provide a relevant discussion in the SM [34] and will address it in the future. Overall, our work further open the door of investigating novel topological phases in the synthetic and real materials.

This work was supported by the Guangdong-Hong Kong Joint Laboratory of Quantum Matter, the NSFC/RGC JRS grant (Grant No. N_HKU774/21), the CRF (Grant No. C6009-20G) and GRF (Grants No. 17310622 and No. 17303023) of Hong Kong, Guangdong Provincial Quantum Science Strategic Initiative (GDZX2200001), and National Key R&D Program of China (Grant No. 2022YFA1405304).

* yqzhuphy@hku.hk
† giandomenico.palumbo@gmail.com
‡ zwang@hku.hk

[1] M. Z. Hasan and C. L. Kane, Rev. Mod. Phys. **82**, 3045 (2010).
[2] X.-L. Qi and S.-C. Zhang, Rev. Mod. Phys. **83**, 1057 (2011).
[3] N. P. Armitage, E. J. Mele, and A. Vishwanath, Rev. Mod. Phys. **90**, 015001 (2018).
[4] D.-W. Zhang, Y.-Q. Zhu, Y. X. Zhao, H. Yan, and S.-L. Zhu, Adv. Phys. **67**, 253 (2018).
[5] N. R. Cooper, J. Dalibard, and I. B. Spielman, Rev. Mod. Phys. **91**, 015005 (2019).
[6] Y. Xu, Frontiers of Physics **14**, 43402 (2019).
[7] T. Ozawa, H. M. Price, A. Amo, N. Goldman, M. Hafezi, L. Lu, M. C. Rechtsman, D. Schuster, J. Simon, O. Zilberberg, and I. Carusotto, Rev. Mod. Phys. **91**, 015006 (2019).
[8] L. Lu, J. D. Joannopoulos, and M. Soljačić, Nature Photonics **8**, 821 (2014).
[9] J. Liu, H. Guo, and T. Wang, Crystals **10**, 305 (2020).
[10] W. Zhu, W. Deng, Y. Liu, J. Lu, Z.-K. Lin, H.-X. Wang, X. Huang, J.-H. Jiang, and Z. Liu, (2023), 10.48550/ARXIV.2303.01426, arXiv:2303.01426 [cond-mat.mes-hall].
[11] M. F. Atiyah, The Quarterly Journal of Mathematics **17**, 367 (1966).
[12] C.-K. Chiu, J. C. Y. Teo, A. P. Schnyder, and S. Ryu, Rev. Mod. Phys. **88**, 035005 (2016).
[13] A. P. Schnyder, S. Ryu, A. Furusaki, and A. W. W. Ludwig, Phys. Rev. B **78**, 195125 (2008).
[14] A. Kitaev, AIP Conf. Proc. **1134**, 22–30 (2009).
[15] P. Hořava, Phys. Rev. Lett. **95**, 016405 (2005).
[16] Y. X. Zhao and Z. D. Wang, Phys. Rev. Lett. **110**, 240404 (2013).
[17] Y. X. Zhao and Z. D. Wang, Phys. Rev. B **89**, 075111 (2014).
[18] W. A. Benalcazar, B. A. Bernevig, and T. L. Hughes, Science **357**, 61 (2017).
[19] Z. Song, Z. Fang, and C. Fang, Phys. Rev. Lett. **119**,

246402 (2017).
[20] J. Langbehn, Y. Peng, L. Trifunovic, F. von Oppen, and P. W. Brouwer, Phys. Rev. Lett. **119**, 246401 (2017).
[21] F. Schindler, Z. Wang, M. G. Vergniory, A. M. Cook, A. Murani, S. Sengupta, A. Y. Kasumov, R. Deblock, S. Jeon, I. Drozdov, H. Bouchiat, S. Guéron, A. Yazdani, B. A. Bernevig, and T. Neupert, Nature Physics **14**, 918 (2018).
[22] F. Schindler, A. M. Cook, M. G. Vergniory, Z. Wang, S. S. P. Parkin, B. A. Bernevig, and T. Neupert, Sci. Adv. **4**, eaat0346 (2018).
[23] H.-X. Wang, Z.-K. Lin, B. Jiang, G.-Y. Guo, and J.-H. Jiang, Phys. Rev. Lett. **125**, 146401 (2020).
[24] S. A. A. Ghorashi, T. Li, and T. L. Hughes, Phys. Rev. Lett. **125**, 266804 (2020).
[25] S. Simon, M. Geier, and P. W. Brouwer, Phys. Rev. B **106**, 035105 (2022).
[26] Q. Wei, X. Zhang, W. Deng, J. Lu, X. Huang, M. Yan, G. Chen, Z. Liu, and S. Jia, Nature Materials **20**, 812 (2021).
[27] S. H. Kooi, G. van Miert, and C. Ortix, Phys. Rev. B **102**, 041122 (2020).
[28] X. Zhang, Z.-K. Lin, H.-X. Wang, Z. Xiong, Y. Tian, M.-H. Lu, Y.-F. Chen, and J.-H. Jiang, Nature Communications **11**, 65 (2020).
[29] Y. Yang, J. Lu, M. Yan, X. Huang, W. Deng, and Z. Liu, Phys. Rev. Lett. **126**, 156801 (2021).
[30] H.-S. Lai, H. Chen, C.-H. Xia, S.-Y. Yu, C. He, and Y.-F. Chen, Research **6**, 0235 (2023).
[31] L. Fu, Phys. Rev. Lett. **106**, 106802 (2011).
[32] Direct calculation for $\mathcal{H}_0$ shows that $C_2 = -\text{sign}(M)$ for $2 < |M| < 4$ and $C_2 = 3\text{sign}(M)$ for $0 < |M| < 2$, and $C_2 = 0$ elsewhere.
[33] X.-L. Qi, T. L. Hughes, and S.-C. Zhang, Phys. Rev. B **78**, 195424 (2008).
[34] See supplemental materials for details.
[35] The inversion symmetry acts on the Hamiltonian as $\hat{\mathcal{I}}\mathcal{H}_0(\boldsymbol{k})\hat{\mathcal{I}}^{-1} = \mathcal{H}_0(-\boldsymbol{k})$ with the represented operator $\hat{\mathcal{I}} = \Gamma_0$.
[36] $\mathcal{M}_i : k_i \to -k_i$ for $i \in (x, y, z, w)$. The operator of $\mathcal{M}_{ij}$ is represented as $\hat{\mathcal{M}}_{ij} = \Gamma_i\Gamma_j$ with $(\hat{\mathcal{M}}_{ij})^2 = -1$.
[37] The high-symmetry points $\Lambda_a^{xw/yz} = (k_x, k_w)/(k_y, k_z) = (0, 0), (0, \pi), (\pi, 0), (\pi, \pi)$ are labeled as $a = 1, 2, 3, 4$ in sequential order.
[38] When $b_{xw} = \pm b_{yw}$, the related combined mirror reflection $\mathcal{M}_{(x\pm y)z} = \mathcal{M}_{x\pm y}\mathcal{M}_z$, where $\mathcal{M}_{x-y} = \mathcal{M}_x C_4^{zw} : (k_x, k_y) \to (k_y, k_x)$, $\mathcal{M}_{x+y} = \mathcal{M}_y C_4^{zw} : (k_x, k_y) \to (-k_y, -k_x)$, with $C_4^{zw} : (k_x, k_y) \to (-k_y, k_x)$ being the four-fold rotation about zw axis. $\mathcal{M}_{(x\pm y)z}$ acts as $(k_x, k_y, k_z, k_w) \to (\mp k_y, \mp k_x, -k_z, k_w)$, represented as $\hat{\mathcal{M}}_{(x\pm y)z} = \frac{1}{\sqrt{2}}(\Gamma_1 \pm \Gamma_2)\Gamma_3$.
[39] The symmetry operators are $\hat{\mathcal{T}} = G_{002}\mathcal{K}$, $\hat{\mathcal{C}} = G_{102}\mathcal{K}$, and $\hat{\mathcal{S}} = \tilde{\Gamma}_6$ satisfying $\hat{\mathcal{T}}^2 = -1$, $\hat{\mathcal{C}}^2 = -1$, and $\hat{\mathcal{S}}^2 = +1$.
[40] When the system hosts $\tilde{\Gamma}_5$ symmetry, we can define a $\mathbb{Z}_2$ number through the spin SCN as $\nu_2 = C_{2s} \bmod 2$ with $C_{2s} = (C_2^+ - C_2^-)/2$ where $C_2^\pm$ is the SCN for each 4×4 block Hamiltonian[41].
[41] Y.-Q. Zhu, Z. Zheng, G. Palumbo, and Z. D. Wang, Phys. Rev. Lett. **129**, 196602 (2022).
[42] The symmetry operators $\hat{\mathcal{I}} = G_{310}$, $\hat{\mathcal{M}}_i = \tilde{\Gamma}_i\tilde{\Gamma}_7$ with $(\hat{\mathcal{M}}_i)^2 = -1$ leading to $\hat{\mathcal{M}}_{ij} = \tilde{\Gamma}_i\tilde{\Gamma}_j$ and $\hat{\mathcal{R}}_i\hat{\mathcal{T}} = \hat{\mathcal{M}}_i\hat{\mathcal{I}}\hat{\mathcal{T}}$ with $(\hat{\mathcal{R}}_i\hat{\mathcal{T}})^2 = +1$ $(i = x, y, z, w)$. For instance, $\hat{\mathcal{R}}_w\hat{\mathcal{T}}$ acting on the Hamiltonian as $\hat{\mathcal{R}}_w\hat{\mathcal{T}}\mathcal{H}_2(k_x, k_y, k_z, k_w)(\hat{\mathcal{R}}_w\hat{\mathcal{T}})^{-1} = \mathcal{H}_2(k_x, k_y, k_z, -k_w)$, where $\hat{\mathcal{R}}_w\hat{\mathcal{T}} = \hat{\mathcal{M}}_w\hat{\mathcal{I}}\hat{\mathcal{T}} = G_{232}\mathcal{K}$.
[43] The spin MFCNs are defined as $C_{1sm}^{ij} = (C_{1m,+}^{ij} - C_{1m,-}^{ij})/2$ for $ij = xw, yz$ with $C_{1m,\pm}^{ij}$ defined in Eq. (2) of each 4×4 block Hamiltonian, respectively.
[44] The system $\mathcal{H}_2$ without SOC now preserves the combined mirror symmetries with the operators $\hat{\mathcal{M}}_{x-y} = \hat{\mathcal{M}}_x\hat{C}_4^{zw} = \frac{1}{\sqrt{2}}(\tilde{\Gamma}_1 - \tilde{\Gamma}_2)\tilde{\Gamma}_7$, $\hat{\mathcal{M}}_{y-z} = \hat{\mathcal{M}}_y\hat{C}_4^{xw} = \frac{1}{\sqrt{2}}(\tilde{\Gamma}_2 - \tilde{\Gamma}_3)\tilde{\Gamma}_7$, $\hat{\mathcal{M}}_{z-x} = \hat{\mathcal{M}}_z\hat{C}_4^{yw} = \frac{1}{\sqrt{2}}(\tilde{\Gamma}_3 - \tilde{\Gamma}_1)\tilde{\Gamma}_7$, where the four-fold rotation symmetry operators $\hat{C}_4^{jw} = \sigma_0 \otimes \sigma_0 \otimes e^{-i\frac{\pi}{4}\sigma_j}$ with $j = x, y, z$.
[45] L. B. Shao and Y. X. Zhao, (2018), 10.48550/ARXIV.1805.07323, arXiv:1805.07323.
[46] K. Wang, J.-X. Dai, L. B. Shao, S. A. Yang, and Y. X. Zhao, Phys. Rev. Lett. **125**, 126403 (2020).
[47] J. Ahn, D. Kim, Y. Kim, and B.-J. Yang, Phys. Rev. Lett. **121**, 106403 (2018).
[48] J.-X. Dai, K. Wang, S. A. Yang, and Y. X. Zhao, Phys. Rev. B **104**, 165142 (2021).
[49] The representative operator of $\mathcal{M}_{(x+z)yw}$ is given by $\hat{\mathcal{M}}_{(z+x)yw} = \hat{\mathcal{M}}_{z+x}\hat{\mathcal{M}}_y\hat{\mathcal{M}}_w = \frac{1}{\sqrt{2}}(G_{223} - G_{221})$ with $(\hat{\mathcal{M}}_{(z+x)yw})^2 = +1$.
[50] Here $C_4^{zw}\mathcal{T}$ acts on $\mathcal{H}_4(\boldsymbol{k})$ as: $(k_x, k_y, k_z, k_w) \to (k_y, -k_x, -k_z, -k_w)$, with $\hat{C}_4^{zw}\hat{\mathcal{T}} = e^{-\frac{\pi}{4}\Gamma_1\Gamma_2}\Gamma_1\Gamma_3\mathcal{K}$ satisfying $(\hat{C}_4^{zw}\hat{\mathcal{T}})^4 = -1$.
[51] C. Wang, A. Hickey, X. Ying, and A. A. Burkov, Phys. Rev. B **104**, 235113 (2021).
[52] S. T. Ramamurthy and T. L. Hughes, Phys. Rev. B **95**, 075138 (2017).
[53] M. R. Hirsbrunner, O. Dubinkin, F. J. Burnell, and T. L. Hughes, (2023), 10.48550/ARXIV.2309.10840, arXiv:2309.10840.
[54] W. Cheng, E. Prodan, and C. Prodan, Phys. Rev. Appl. **16**, 044032 (2021).
[55] S. Ma, Y. Bi, Q. Guo, B. Yang, O. You, J. Feng, H.-B. Sun, and S. Zhang, Science **373**, 572 (2021).
[56] Z.-G. Chen, W. Zhu, Y. Tan, L. Wang, and G. Ma, Phys. Rev. X **11**, 011016 (2021).
[57] H. Chen, H. Zhang, Q. Wu, Y. Huang, H. Nguyen, E. Prodan, X. Zhou, and G. Huang, Nature Communications **12**, 5028 (2021).
[58] Y. Wang, H. M. Price, B. Zhang, and Y. D. Chong, Nature Communications **11**, 2356 (2020).
[59] Z. Wang, X.-T. Zeng, Y. Biao, Z. Yan, and R. Yu, Phys. Rev. Lett. **130**, 057201 (2023).
[60] H. Price, O. Zilberberg, T. Ozawa, I. Carusotto, and N. Goldman, Physical Review Letters **115**, 195303 (2015).
[61] I. Petrides, H. M. Price, and O. Zilberberg, Phys. Rev. B **98**, 125431 (2018).
[62] M. Lohse, C. Schweizer, H. M. Price, O. Zilberberg, and I. Bloch, Nature **553**, 55 (2018).
[63] J.-B. Bouhiron, A. Fabre, Q. Liu, Q. Redon, N. Mittal, T. Satoor, R. Lopes, and S. Nascimbene, Science **384**, 223 (2024).
[64] H. Zhang, C.-X. Liu, X.-L. Qi, X. Dai, Z. Fang, and S.-C. Zhang, Nature Physics **5**, 438 (2009).
[65] Y. L. Chen, J. G. Analytis, J.-H. Chu, Z. K. Liu, S.-K. Mo, X. L. Qi, H. J. Zhang, D. H. Lu, X. Dai, Z. Fang, S. C. Zhang, I. R. Fisher, Z. Hussain, and Z.-X. Shen,

Science **325**, 178 (2009).

[66] The perturbation term $\Delta_1 = b_{xw} G_{01} + b_{yw} G_{02}$ can be induced by (i) magnetization with the Zeeman Hamiltonian as $H_Z = \sigma_0 \otimes (\mathbf{B} \cdot \boldsymbol{\sigma})$ where an effective magnetic field $\mathbf{B} = (b_{xw}, b_{yw}, 0)$;(ii) a Floquet periodic driving $H_d(t) = \cos\omega t(A_x G_{02} + A_y G_{01}) + A_w \sin\omega t G_{03}$ with the Floquet Hamiltonian in the high-frequency limit [70], up to the first-order in $1/\omega$, being $H_F = \frac{A_w}{i\omega} G_{03}(A_x G_{02} + A_y G_{01}) = \Delta_1$.

[67] Z. Gong, Y. Ashida, K. Kawabata, K. Takasan, S. Higashikawa, and M. Ueda, Phys. Rev. X **8**, 031079 (2018).

[68] S. Yao and Z. Wang, Phys. Rev. Lett. **121**, 086803 (2018).

[69] J. Cayssol, B. Dóra, F. Simon, and R. Moessner, physica status solidi (RRL)–Rapid Research Letters **7**, 101 (2013).

[70] N. Goldman and J. Dalibard, Phys. Rev. X **4**, 031027 (2014).